HHS Public Access

Author manuscript

Biomaterials. Author manuscript; available in PMC 2017 January 01.

Published in final edited form as:

Biomaterials. 2016 January ; 75: 260–270. doi:10.1016/j.biomaterials.2015.10.031.

Matrix metalloproteinase-20 mediates dental enamel biomineralization by preventing protein occlusion inside apatite crystals

Saumya Prajapati[a], **Jinhui Tao**[b], **Qichao Ruan**[a], **James J. De Yoreo**[b], and **Janet Moradian-Oldak**[a,*]

[a]University of Southern California, Herman Ostrow School of Dentistry, Division of Biomedical Sciences, Center for Craniofacial Molecular Biology, Los Angeles, CA 90033, USA

[b]Physical Sciences Division, Pacific Northwest National Laboratory, Richland, WA 99352, USA

Abstract

Reconstruction of enamel-like materials is a central topic of research in dentistry and material sciences. The importance of precise proteolytic mechanisms in amelogenesis to form a hard tissue with more than 95% mineral content has already been reported. A mutation in the Matrix Metalloproteinase-20 (MMP-20) gene results in hypomineralized enamel that is thin, disorganized and breaks from the underlying dentin. We hypothesized that the absence of MMP-20 during amelogenesis results in the occlusion of amelogenin in the enamel hydroxyapatite crystals. We used spectroscopy and electron microscopy techniques to qualitatively and quantitatively analyze occluded proteins within the isolated enamel crystals from MMP-20 null and Wild type (WT) mice. Our results showed that the isolated enamel crystals of MMP-20 null mice had more organic macromolecules occluded inside them than enamel crystals from the WT. The crystal lattice arrangements of MMP-20 null enamel crystals analyzed by High Resolution Transmission Electron Microscopy (HRTEM) were found to be significantly different from those of the WT. Raman studies indicated that the crystallinity of the MMP-20 null enamel crystals was lower than that of the WT. In conclusion, we present a novel functional mechanism of MMP-20, specifically prevention of unwanted organic material entrapped in the forming enamel crystals, which occurs as the result of precise amelogenin cleavage. MMP-20 action guides the growth morphology of the forming hydroxyapatite crystals and enhances their crystallinity. Elucidating such molecular mechanisms can be applied in the design of novel biomaterials for future clinical applications in dental restoration or repair.

Keywords

Matrix metalloproteinase-20; Protein occlusion; Enamel biomineralization; Amelogenin

*Corresponding author. joldak@usc.edu (J. Moradian-Oldak).

1. Introduction

Nature provides us with many examples of biominerals, including calcium phosphate crystals in bones and teeth, and calcium carbonate crystals in nacre and sea urchins [1]. A very fundamental part of biomineralization is the complex extracellular macromolecular framework in which mineralization occurs, such as the collagen fibrils in bone and dentin, polysaccharides in nacre and extracellular matrix proteins in dental enamel. Macromolecules such as proteins, glycoproteins and enzymes regulate the process of mineral nucleation and growth in various ways to create biomaterials with outstanding mechanical properties [2]. These macromolecules can interact with ions to stabilize the amorphous phase prior to crystal formation, adsorb on particular crystal faces and stabilize certain polymorphs [3,4]. Moreover, they can be adsorbed on edges and terraces of crystals to promote growth in a certain direction and therefore control crystal morphology [5–8]. In the case of the sea urchin, these macromolecules become overgrown following adsorption and are occluded within the crystal [9]. The occlusion of these molecules can affect the crystal texture and cause morphological changes, consequently affecting the mechanical properties of the mineral [10–12].

Enamel is the outermost layer of the tooth and is the hardest bioceramic in the vertebrate body. It consists of highly organized hydroxyapatite (HAP) crystals. Enamel formation (amelogenesis) is a highly orchestrated process that involves precise cell signaling mechanisms, secretion, assembly and degradation of enamel matrix proteins [13,14]. Although the process of enamel biomineralization occurs in an extracellular matrix enriched in proteins, mature enamel crystals have virtually no organic content [15]. Mature enamel contains only 1–2% organic material that is mostly concentrated at the periphery of the prism bundles [16,17] Two major stages of amelogenesis, namely the secretory and maturation stages, have been defined according to the morphology and function of ameloblasts [18]. Enamel formation begins during the secretory stage with the ameloblast cells laying down an organic matrix followed by immediate and simultaneous nucleation of amorphous calcium phosphate mineral in the form of long, thin ribbons adjacent to the secretory faces of ameloblasts [18–20]. The matrix secreted into the future enamel space consists of several proteins, including amelogenin, enamelin, ameloblastin and amelotin, along with proteases such as Matrix Metalloprotinease-20 (MMP-20) and Kallikrein-4 (KLK-4). MMP-20 is secreted during the secretory stage and is involved in cleavage of specific domains in enamel matrix proteins [21–23]. Enamel biomineralization is completed at the maturation stage when KLK-4 is secreted to completely digest the extracellular matrix, resulting in hardening of the tissue by allowing the enamel apatite crystallites to grow mostly in thickness and fill the space.

MMP-20 is critical for normal enamel formation, as several mutations in the MMP-20 gene in humans have been reported to cause Amelogenesis Imperfecta (AI), a hereditary disease of enamel malformation [24,25]. The affected teeth present with a hypo-maturation phenotype showing pigmentation, mottling, roughness, brittleness and sometimes fracture of the enamel. The MMP-20 null mouse was created to study the effects of MMP-20 on enamel formation by deleting the majority of exons 4 and 5 of the MMP-20 gene [26]. The resulting phenotype is associated with several defects in the enamel: hypoplasia (thin enamel),

hypomineralization (soft enamel) with an altered enamel rod pattern, enamel that breaks off from the dentin, an absence of the characteristic decussating pattern and deteriorating enamel morphology [26]. The MMP-20 null mouse also shows a large number of enamel-free areas in the maxillary molars when observed under SEM [26,27].

In the present study, we took advantage of the MMP-20 null mouse as a model to study the effect of this metalloproteinase on the nucleation and growth morphology of enamel HAP crystals by analyzing individual isolated apatite crystals from the two major stages of enamel formation. We hypothesized that in MMP-20 null mice, amelogenin and other enamel matrix proteins are trapped inside the hydroxyapatite crystals during the secretory stage of amelogenesis, affecting the growth and maturation of these crystals. Our hypothesis was based on our recent finding that the full-length amelogenin protein is occluded inside calcite crystals grown *in vitro* in the absence of MMP-20. The presence of amelogenin in the crystallization solution resulted in pits and steps on the calcite crystal surface, but the morphology of the crystals was rescued following the addition of MMP-20 to the crystallization solution. Our *in vitro* study suggested that, along with its other proposed functions, MMP-20 may prevent protein occlusion inside apatite crystals during enamel formation [28]. We combined electron microscopy and atomic force microscopy techniques to analyze morphology of isolated enamel crystals from MMP-20 null mice and ascertain whether proteins were present inside the HAP crystals. We present evidence that supports a novel function of a metalloproteinase in calcium phosphate biomineralization and provides insight into the question of why extracellular proteins need to be cleaved. Understanding the molecular mechanisms that govern the physiological function of MMP-20 in mediating crystal formation is important for future development of a biomimetic enamel-like material [29–31]. Such a material would have a great potential as an alternative dental restorative material for repairing damaged human tooth enamel [32].

2. Materials and methods

2.1. Animals

MMP-20 heterozygous mice (MMP-$20^{+/-}$) with a C57BL/6J background were obtained from the Mutant Mouse Regional Resource Center (MMRC) and housed in the University of Southern California Vivarium. This study was approved by the University of Southern California Institutional Animal Care and Use Committee.

2.2. Enamel crystal isolation

The MMP-20 heterozygous mice were mated to obtain MMP-$20^{+/+}$ and MMP-$20^{-/-}$ colonies. The MMP-$20^{+/+}$ males and females were mated to obtain WT colonies which were used as controls in this study. The MMP-$20^{-/-}$ males and females were mated to obtain MMP-20 null mice, which were used for all the experiments. The females were checked for vaginal plugs every day. The pups were weaned at the age of three weeks and were also tagged and genotyped at this age. Genotyping was performed by Transnetyx using the following primers: MMP-20 null 5′GCCGAGGATTTGGAAAAAGTGTTTA3′ and 3′TTCATGACATCTCGAGCAAGTCTTT5′and WT 3′ATACCCCAAAAAGC ATGAAGAGACT3′and 3′CAAGTTTTAAAGGTTGGTGGGTTGT5′. Mandibular and

maxillary incisors from adult MMP-20 null and WT mice were dissected. The incisors were depulped and cleaned in simulated enamel fluid (SEF) by sonicating them 3 times in a water bath for 30 s each, with a one minute interval in between each sonication. The SEF was changed each time. The incisors were air-dried and the secretory-stage enamel was isolated using a scalpel and collected in pre-weighed tubes. The WT incisors were freeze-dried for 12 h before the isolation of the maturation-stage enamel. Maturation-stage enamel from the MMP-20 null mice was easily removed by scraping it with a scalpel and was therefore not freeze-dried prior to isolation.

2.3. Amelogenin preparation

Recombinant mouse amelogenin rM179 was expressed and purified as previously described [33]. The amelogenin obtained through this procedure is an analogue to M180 but lacks the first methionine and is non-phosphorylated.

2.4. Extraction of intra-crystalline enamel proteins

The isolated enamel was weighed and washed with a series of protein extraction buffers, specifically phosphate buffer (0.1 M pH 7.4) and tris urea buffer (50 mM Tris+ 4 M Urea pH 7.4), as shown in Fig. 1. These washes removed all the adsorbed proteins from the enamel surface and were followed by washes with distilled water to remove the remaining buffer. The supernatant was collected each time and stored for further evaluation. The enamel crystals were then dissolved in 1 M HCl. Supernatants collected from the second wash with Tris Urea buffer (W1UT, W2UT and W3UT) and dissolved crystals (W1HCl) were desalted using a Microcon Centrifugal Filter Devices MW: 3000 Da at 10,000 rpm for 40 min at 4 °C. They were then freeze-dried and reconstituted in 200 μl of distilled water for further analysis.

2.5. Quantitative analysis of intra-crystalline proteins using UV-absorption and Western Blot

Supernatants collected from each wash, as described in Fig. 1 were either dialyzed before freeze-drying or directly freeze-dried. Protein was quantified from all the supernatants obtained as shown in Fig. 1 using a Nanodrop ND-1000 spectrophotometer (NanoDrop Products, Wilmington, DE) at $\lambda = 280$ nm. The supernatants were dissolved in 1X loading buffer, loaded in 12% acrylamide gels and run at 120 V. One gel was used for silver staining and the second gel was used for Western Blot. The gel was transferred to a PVDF membrane using a wet transfer at 120 V for 1 h, incubated with 5% non-fat milk in PBST (0.01% Tween-20), immunostained with primary antibody and then visualized using an enhanced chemiluminescence plus Western blotting detection system (GE Healthcare). The antibody used was a polyclonal antibody raised against recombinant mouse amelogenin (rM 179) in chicken [34].

2.6. SEM and TEM sample preparation

Enamel crystals isolated from adult incisors of MMP-20 null and WT mice as described earlier (Fig. 1, step 4) were analyzed using Scanning Electron Microscopy (SEM) and High Resolution Transmission Electron Microscopy (HR-TEM). The enamel crystal samples for

SEM were suspended in 100% ethanol and placed on SEM mounts. They were gold-plated for 30 s and imaging was performed in a field emission scanning electron microscope (JEOL JSM-7001F) operating at an accelerating voltage of 10 keV.

The samples for HR-TEM were suspended in 100% ethanol, placed on TEM grids (Carbon Type-B, Ted Pella Inc.) and dried for at least 14 h before imaging. HR-TEM images were obtained on a JEOL JEM-2100 microscope using an accelerating voltage of 200 keV.

2.7. Raman spectroscopy

Micro-Raman spectroscopy was used to investigate the presence of associated organic materials as well as to determine the crystallinity of isolated enamel crystals of WT and MMP-20 null mouse enamel, at both the secretory and maturation stages. Samples were prepared as described in Fig. 1. The Raman spectra were collected from 100 to 4000 cm^{-1} under backscattering geometry by a LabRAM ARAMIS confocal Raman Microscope (HORIBA scientific, Japan) operated at a resolution of 2 cm^{-1} with an excitation wavelength of 532 nm and laser power of 2.5 mW. A × 60 objective with numerical aperture of 0.75 was used to focus the sample and to collect the spectra for 20 s. The experiment was repeated 5 times for each sample and the results were averaged.

To evaluate the relative crystallinity of enamel crystals of WT and MMP-20 null animals in both secretory and maturation stages, the Raman peak of totally symmetric stretching mode (ν_1) of the PO_4 group located at ~960 cm^{-1} was used for FWHM analysis [35]. Gaussian functions of the form:

$$f(x)=y_0+\frac{A}{\sigma\sqrt{2\pi}}e^{-(x-\mu)^2/(2\sigma^2)}$$

where y_0 is the intensity at the base of the peak, μ is the x coordinate (cm^{-1} by Raman shift) at the center of the peak, A is the area of the peak, and σ is the standard deviation or Gaussian RMS width. Gaussian Function was used to fit the Raman peak at 960 cm^{-1} with convergence of the R^2 = 0.99 by Origin 8.5 (Origin Lab Corporation). In this case, the FWHM was equal to $2\sqrt{2\ln 2}\sigma$.

2.8. Atomic force microscopy (AFM)

2.8.1. Crystal thickness measurements—A muscovite mica disc (diameter 9.9 mm, Ted Pella, Inc.) was freshly cleaved and used as a supporting surface. The mica surface was washed with 50 μl poly-L-lysine solution (0.1% w/v, Ted Pella) for 5 min, thoroughly rinsed with water and dried by a stream of nitrogen gas. WT and MMP-20 null enamel crystals from the maturation and secretory stages were prepared as described in Fig. 1, and then dispersed in water by sonication for 10 min to prevent aggregation of the crystals. Three μl of this suspension was placed on the poly-L-lysine functionalized mica. To measure the thickness of the enamel crystals, all samples were imaged in air by a NanoScope 8 Atomic Force Microscope equipped with a J scanner. The images were captured in tapping mode with silicon tips (PPP-FMR rectangular cantilever, nominal spring constant k = 2 N/m, tip radius <10 nm, resonance frequency 75 kHz in air, Nanosensors™). Cantilevers were

resonated at approximately 75 kHz with a free amplitude of 50 nm, and images were collected at a tapping amplitude of approximately 80% of free amplitude. All the width and thickness values were determined manually from the images using NanoScope Analysis 1.4 software and the histogram was plotted by Origin 8.5 (OriginLab Corporation).

2.8.2. Force curves—The fixation of samples on the surface was the same as described above for thickness measurements. Thereafter both the enamel crystals and AFM cantilever were treated with plasma to remove residual organic material adsorbed on the surface. Time-lapse AFM images were continuously collected in an AFM equipped with a fluid cell after thermal relaxation for 10 min.

All *in situ* AFM images were captured in ScanAsyst mode at room temperature (23 °C) with a NanoScope 8 Atomic Force Microscope (E scanner, Bruker) using silicon nitride tips (TR400PSA triangular lever; k = 0.08 N/m; tip radius ~20 nm; resonance frequency 34 kHz in air; Asylum Research, Inc.). The signal-to-noise ratio was maintained above 10. The scanning speed was 1–2 Hz. The peak force set point was carefully tuned to minimize the average loading force (~50 pN) during *in situ* imaging. Force curves between the silicon nitride tips and enamel crystals were measured in order to determine the organic material trapped inside the crystals. Force curves were collected after etching the outer surface of WT and –20 null enamel crystals with 200 μl HCl at pH 4.6 followed by washing with 400 μl of water. The measurements before and after etching were performed in water. A constant approach and retraction velocity of 500 nm/s and dwell time of 1 s were used and more than 50 individual force curves were collected for each surface condition. The average adhesion force was used to determine the organic content.

2.9. Statistical analysis of the areas of imperfection in the crystals

All statistical analysis for Fig. 8E was performed in Microsoft Excel 2010. The significance level was calculated by performing unpaired T-tests assuming unequal variances with $p < 0.05$. The imperfections were calculated by taking a Fourier Transformation (FFT) of areas of interest (AOI) of dimensions $8.4 \times 8.4\ nm^2$. The FFT was calculated for each AOI using Digital Micrograph software. AOIs showing no discernable diffraction pattern in the FFT were calculated as regions of imperfections. All such AOIs from 6 different crystals (1 from secretory stage, 2 from maturation stage and 3 mixed populations) from both WT and MMP-20 null mice were calculated and averaged.

3. Results and discussion

3.1. Qualitative and quantitative analysis of occluded proteins inside the enamel crystals of MMP-20 null mice

Fig. 2 shows the SDS-PAGE and Western blot analysis of proteins extracted from WT and −20 null mouse enamel crystals. The SDS-PAGE analysis showed a decrease in the amount of adsorbed proteins on the enamel crystals collected from secretory and maturation stages with each extraction buffer wash (Lanes 1–6, Fig. 2A & B). Washes W1UT and W2UT showed the maximum number of bands on the gel due to the presence of 4 M urea in the extraction buffer. The last washes, W2P′ and W3P′, showed no protein bands, which

indicates that all the adsorbed proteins from the enamel crystals had been washed off (Lanes 5 and 6, Fig. 2A & B). The crystals dissolved in W1HCl in the MMP-20 null mouse showed a band corresponding to the full-length amelogenin (M180), which was confirmed by Western Blot (data not shown). The amount of intra-crystalline proteins recovered in the W1HCl wash were also calculated using a Nanodrop at $\lambda = 280$ nm (UV-absorption). Remarkably, the total amount (normalized) of proteins in the MMP-20 null crystals was almost 4 times what was found in the WT mice (Fig. 2C).

Since MMP-20 is expressed during the secretory stage of amelogenesis, the enamel crystals from secretory and maturation stages for WT and MMP-20 null mice were evaluated separately in order to investigate the function of −20 (Western blot in Fig. 2D). All the samples were washed with the extraction buffers as shown in Fig. 1. Lanes 1 and 2 represent the samples from the secretory-stage crystals of −20 null and WT mice, respectively. The amount of protein observed in the MMP-20 null mouse was more than the WT mice as also shown in previous findings [36]. Lane 2 showed some proteins, which was expected because it represents an early stage of enamel formation during which some enamel matrix proteins are still retained. Lanes 5 and 6 represent the maturation-stage crystals of −20 null and WT mice, respectively. −20 null mice showed the presence of full-length amelogenin even at this stage, whereas in the WT mice the amount of retained proteins was almost negligible. The WT mice showed no band in the Western blot, which indicated that the mature enamel had no retained amelogenin (Fig. 2D). The amount of intra-crystalline proteins calculated using UV-adsorption (Fig. 2E) showed a similar trend to the Western blot (Fig. 2D). MMP-20 null mice at the secretory stage had the highest amount of proteins whereas the WT maturation stage had very small amounts compared to MMP-20 null mice.

Our present data corroborate an earlier report that the amount of volatiles (proteins and water) at the maturation stage in MMP-20 null enamel was almost twice the amount detected in the wild type [36]. The differences between our observations and those in previous studies could be due to the difference in the processing of the tissue. In the previous study, enamel strips of 1 mm each were used to measure the mineral and protein content, whereas we used bulk-scraped enamel to make our measurements. Here we demonstrate that the amount of proteins in the MMP-20 null enamel is higher even during the secretory stage, most likely due to the lack of protein degradation and entrapment of mostly full-length amelogenin in the crystals at this early stage. The excess amount of amelogenin seen at the maturation stage (lane 5 in Fig. 2D & E) in the MMP-20 null mouse indicates that MMP-20 is an important proteinase and amelogenesis is affected by its absence even though a digestive enzyme such as KLK-4 is secreted during the maturation stage [37]. Based on our findings, we hypothesize that the ineffectiveness of KLK-4 in digesting amelogenin proteins in MMP-20 null mice is the result of amelogenin entrapment inside the secretory-stage enamel crystals. Further studies are needed to address this hypothesis.

We also performed Raman Spectroscopy in order to confirm the presence of organic material inside MMP-20 null mouse enamel crystals (Fig. 3). At the secretory and maturation stages, the MMP-20 null enamel crystals showed the presence of a broad peak at 3000 cm^{-1}, which corresponds to the C–H vibrational ring and is indicative of organic

material in the sample. The Raman results are also consistent with the Western blot and UV-adsorption findings (Fig. 2D – E). In our previous *in vitro* study with calcite, similar organic peaks were observed in the calcite crystals grown in the presence of amelogenin without MMP-20 in the crystallization solution [28]. This also indicates that failure to degrade amelogenin can cause retention of these proteins within the crystals.

The presence of intra-crystalline proteins in enamel crystals isolated from MMP-20 null mice was further analyzed by AFM force spectroscopy to measure the adhesive forces between the silicon nitride tip and the surface of the sample before and after the dissolution of the crystals with HCl at pH 4.6 (Fig. 4) [38]. Fig. 4A shows the typical force curves that were obtained for WT and MMP-20 null enamel crystals at both secretory and maturation stages. It shows the presence of single and multiple rupture forces in MMP-20 null secretory (Fig. 4I & J), maturation (Fig. 4 E & F) and WT secretory stage (Fig. 4G & H) enamel crystals before and after dissolution with HCl. In contrast, the WT maturation stage (Fig. 4C & D) enamel crystals showed only a single rupture force curve before and after dissolution with HCl. Multiple rupture force curves are an indication of interaction between the Si_3N_4 tip and stretchable macromolecules such as proteins or polysaccharides [39,40]. The percentage of multiple rupture force curves out of the total number of curves measures the probability of the tip picking up the organic material on the surface or on the newly exposed surface after acid etching. The results (Fig. 4B) show a significant increase in the percentage of multiple rupture force curves after acid etching in enamel crystals from the WT secretory stage, MMP-20 null secretory and maturation stages, indicating the presence of some occluded organic macromolecules inside the enamel crystals in these samples. Amelogenin and other enamel matrix proteins may act as nucleation centers for unseeded crystallization when present in small quantities but may inhibit crystal growth when present in larger quantities [41]. In the case of the MMP-20 null mouse, an excess of enamel matrix proteins, mainly the full-length amelogenin that remains due to the absence of MMP-20, may cause retention of amorphous calcium phosphate and inhibition of crystal growth or phase transformation [42]. Similar results have also been shown previously in the growth of calcite crystals in the presence of abalone nacre proteins [43].

3.2. The isolated enamel crystals of MMP-20 null mice have abnormal size and morphology

Differences in enamel crystal size and morphology between WT and MMP-20 null mice were observed using TEM, SEM and AFM. There was a stark difference between the WT (Fig. 5A) and MMP-20 null enamel crystals (Fig. 5E) when observed under TEM. The WT (Fig. 5A) crystals were long and showed dark bands which, as reported earlier, were due to differences in density caused by slight bends, leading to oblique views that create the appearance of these band-like regions [44]. No dark bands were observed in the MMP-20 null enamel crystals (Fig. 5E) which may be the result of the decrease in the length of the crystals. The MMP-20 null enamel crystals appeared more plate-like compared to those of the WT.

Previous SEM studies of MMP-20 null mice have shown an absence of the typical decussating pattern and an increase in proteins associated with enamel crystals [26]. In our study, the isolated enamel HAP crystals of MMP-20 null mice (Fig. 5F) were more

heterogeneous and showed an overall decrease in length compared to the WT (Fig. 5B) controls. They also appeared wider and thinner than in the WT. The enamel crystals of MMP-20 null mice were difficult to isolate because of the amount of proteins associated with them. Previously it was shown that the addition of mineral ions to maturation-stage enamel crystals did not cause any growth in the crystals until the residual proteins were removed by 8 M urea or sodium hypochlorite [45]. This shows the importance of protein processing by MMP-20 and demonstrates how the length of the enamel crystals may be affected by the excess retention of enamel matrix proteins.

Systematic analysis of the size distribution of isolated maturation-stage enamel crystals from WT and MMP-20 null mice was performed by AFM (Fig. 5C–D&G–H). The histogram was calculated using 137 dispersed crystals from WT mice and 28 crystals from MMP-20 null mice, and shows the difference in the width and thickness of these crystals. The width of the majority of WT enamel crystals ranged from 50 to 90 nm (Fig. 5C) whereas the MMP-20 null enamel crystals had a wide distribution in size, with the majority ranging from 60 to 120 nm (Fig. 5G). The MMP-20 null crystals also showed a slight decrease in thickness (Fig. 5D), with most crystals ranging from 20 to 30 nm, whereas the majority of WT crystals ranged from 20 to 40 nm (Fig. 5H).

The effect of amelogenin on the morphology of OCP crystals, used as a model for enamel apatite crystals, was previously reported in an *in vitro* study. The length-to-width ratio of OCP crystals increased in the presence of the degradation product of −20 action, namely mouse amelogenin lacking the c-terminal (rM166), as compared to the controls. It was reported that following the interactions of truncated amelogenins with the hydrophobic (010) faces of OCP, the width-to-thickness ratio in the presence of rM166 as well as the presence of extracted bovine amelogenins decreased as compared to the controls [46]. These studies together with our present findings support the notion that the timely processing of amelogenin and possibly other enamel proteins by MMP-20 is important for the proper growth morphology and maturational volumetric expansion of the enamel crystals. We therefore suggest that step-wise processing of amelogenin by MMP-20 determines the growth morphology of enamel crystals. Whether the presence of occluded organic material or amorphous calcium phosphate (ACP) can affect the overall growth morphology of enamel crystals is a subject left for future investigation. However, the presence of organic material occluded in the enamel crystal lattice may affect the crystallinity and the lattice periodicity [10–12].

The crystal lattice patterns of the isolated WT and MMP-20 null enamel crystals were observed using HR-TEM (Fig. 6). In agreement with our SEM study (Fig. 5), MMP-20 null enamel crystals (Fig. 6D) appeared shorter in length, thinner and more plate like than those of the WT (Fig. 6A). Panels 6B and 6E show higher-magnification views of individual crystals from WT and MMP-20 null mice, respectively. The insets in these panels show the diffraction pattern of the highlighted region created by Digital Micrograph (DM) 2.30.542.0 software. Based on the 002 and 004 diffraction, the patterns were typical of hydroxyapatite, as shown previously [44,47]. Panels 6C (10×10 nm^2) and 6F (10×10 nm^2) show high-resolution views of the highlighted areas in Fig. 6B and E, respectively. The WT enamel crystal (Fig. 6C) shows a pattern characteristic of HAP crystal lattice. A similar pattern can

be observed in the enamel from −20 null mice (Fig. 6F), but notably there is also an area showing an absence of the lattice pattern (highlighted by dotted lines). This is an example of the imperfections that are present throughout the HAP crystals in MMP-20 null mice.

3.3. The crystallinity of MMP-20 null enamel is affected

The full width of half maximum (FWHM) of the peak in totally symmetric stretching mode (ν_1) of the tetrahedral PO_4 at 960 cm^{-1} is used as a measure of crystallinity inside apatite crystals (Fig. 7). The lower FWHM shows that the WT enamel had higher crystallinity than −20 null enamel and that the maturation-stage enamel had higher crystallinity than the secretory stage enamelin both WT and −20 null mice.

HR-TEM images (Fig. 8A – D) show different types of defects in the enamel crystals of MMP–20 null mice. The sudden loss of lattice pattern in a single crystal is shown in Fig. 8A and B, as indicated by the arrows. We interpret these lattice imperfections to be the result of the presence of occluded enamel matrix proteins or the presence of amorphous calcium phosphate, or both. Studies have shown that the enamel HAP crystals form through an intermediate stage of ACP and *in vitro* studies have demonstrated that the full-length amelogenin stabilizes ACP and prevents its transformation into HAP [4,20,48]. Fig. 8C and D shows misalignment in the lattice intervals in a single enamel crystal. Such misalignments could also be a result of protein occlusion inside these crystals. These misaligned areas showed an absence of a diffraction pattern when a Fourier Transform (FFT) was performed on a single crystal using Digital Micrograph software. We calculated the areas of such imperfections in the MMP-20 null mice and compared them to the areas of imperfections in the WT mice. Remarkably, the MMP-20 null mice showed imperfections covering 31% of the area, as compared to 10% in the WT mice, which is a statistically significant difference (Fig. 8E). The observation that full-length amelogenin M180 was occluded within the crystals in −20 null mice (Fig. 2) supports the notion that both protein and ACP could coexist in the areas of imperfections in the crystals (Fig. 8A&B).

In vitro studies have shown that the full-length amelogenin stabilizes calcium phosphate clusters and forms a metastable ACP-amelogenin complex which ultimately transforms into HAP [49]. The presence of a transient ACP phase at early stages of enamel formation was also demonstrated by Beniash [20]. The interaction of the hydrophilic carboxyl-terminal in the full-length amelogenin with calcium phosphate ions is important for the function of amelogenin to interact with apatite crystal surfaces and stabilizing the ACP phase. Therefore, it was hypothesized that cleavage of this C-terminal may promote the phase transformation from ACP to apatite, which ultimately fuses together to form hard enamel [4].

Certain amino acids, like aspartic acid, adopt a β sheet structure after binding to Ca^{2+} ions, which makes it easier for the protein to interact with a certain phase of the crystal [41,50]. In the case of amelogenin it was shown that certain regions of the protein adopt a β sheet structure when they come in contact with HAP crystals [51]. This could result in the occlusion of full-length amelogenin within the crystal if not cleaved on time by the MMP-20. We have shown previously that the hydrophilic c-terminal of amelogenin interacts strongly with apatite crystals [52]. The full-length amelogenin may become trapped inside

the growing crystals because the proteins have a tendency to adhere to the crystals [52]. In the absence of MMP-20, full-length amelogenin is retained, which makes it easier for the protein to become occluded within the enamel crystal.

Tao et al. also showed that during the transformation of ACP to HAP in the presence of glycine and glutamic acid, these amino acids were expelled from the interior of the crystals [53]. Although it is not yet clear whether this is the case *in vivo*, the notion that small peptides resulting from the degradation of enamel matrix proteins could be expelled from the crystals during mineralization cannot be eliminated, and the presence of amelogenin in MMP-20 null enamel crystals as well as the absence of amelogenin in the WT (Fig. 2) strongly support this idea.

Previous studies have elucidated the roles of enzymes in bio-mineralization. In an *in vivo* study it was shown that alkaline phosphatase (ALP) plays a role in the initiation of mineralization by aiding the maturation of organic matrix protein during the shell formation of European abalone [54]. *In vitro* study demonstrated that ALP mediated the mineralization of a peptide matrix in the presence of β-glycerophosphate. It was further shown that ALP induces mineral formation by hydrolyzing the heavily phosphorylated matrix and releasing phosphate ions [55]. In the present study we propose a new function of enzymes in biomineralization and in particular demonstrate that MMP-20 guides HAP formation during amelogenesis by altering amelogenin biochemistry and hence its effect on mineral formation.

Our systematic comparison of enamel crystals isolated from WT and MMP-20 null mice may shed some light on the mechanisms of enamel crystal formation at a molecular level. The presence of full-length amelogenin and crystal lattice defects in the maturation-stage enamel of MM-20 null mice shows that the stepwise cleavage of the hydrophilic c-terminal of amelogenin is crucial to the growth morphology and high crystallinity of enamel crystals. Another protease; KLK-4 which is secreted in the maturation stage in these mice is not able to compensate completely for the loss of MMP-20, which shows that the initial processing of enamel matrix proteins by MMP-20 is a prerequisite for the complete degradation by KLK-4. The interplay between organic and inorganic molecules in enamel formation is crucial to its unique structural and mechanical properties [41]. We demonstrate that amelogenin processing by MMP-20 is crucial for complete mineralization of the enamel. An *in vitro* study showed that MMP-20 processing of amelogenin accelerates mineralization and promotes crystal growth [56]. Therefore, in the case of MMP-20 null mice, the absence of MMP-20 can inhibit the rate of mineralization, preventing the enamel crystals from maturing properly. Ameloblastin and enamelin are major non-amelogenins which are important for enamel formation. In our previous *in vitro* studies we have reported that cooperative interaction between the 32 kDa enamelin and amelogenin regulated the growth of octacalcium phosphate (OCP) crystals. The presence of enamelin also increased the aspect ratio of the OCP crystals [57,58]. The presence of enamelin or ameloblastin was not analyzed in our study. However, we cannot rule out their role in enamel crystal formation and hence the possibility that they are present in the areas of imperfections in the crystals along with amelogenins.

Because dental enamel does not regenerate itself, developing strategies to mimic dental enamel is of significant importance for clinical applications. Several studies have attempted to grow artificial enamel, which could be used to fill clinical defects or pathologies involving enamel. We have recently demonstrated that a biomimetic amelogenin hydrogel could promote the formation of enamel-like co-aligned crystals [29]. The repaired enamel showed a remarkable improvement in its mechanical properties, though they were still not on par with natural enamel. Beniash et al. have reported that enamel from MMP-20 null mice was about 37% softer than normal enamel. The biggest difference in mineralization observed in that study between control and MMP-20 null mice was in mature enamel [27]. Our study provides an improved understanding of enamel HAP formation and the role of MMP-20 in this process. It also shows that the degradation of enamel matrix proteins in the secretory stage prevents occlusion of these proteins in the HAP crystals. Although we have been able to "re-grow" enamel-like layers *in vitro*, in the future, we can use the strategy of implementing proteinases, to mimic the natural process and "re-grow" a biomimetic layer with improved mechanical properties.

4. Conclusions

We used biochemical, spectroscopy and imaging techniques to provide evidence that amelogenin was occluded inside the enamel crystals isolated from MMP-20 null mice, resulting in their abnormal size and morphology. The MMP-20 null enamel crystals were smaller in size, wider and thinner in shape, and had more areas of imperfections inside them when compared to those of the WT. The MMP-20 null mice had almost 4 times the protein associated with their enamel crystals than the WT. The occlusion of amelogenin inside the MMP-20 null crystals decreased their crystallinity. All these findings support the notion that MMP-20 is a crucial enzyme during the process of amelogenesis that controls the HAP crystal formation by degrading the enamel matrix proteins, the absence of which affects the overall morphology and crystallinity of enamel crystals. Our systematic approach to studying the enamel secretory- and maturation-stage crystals can also be used in other animal models in which enamel matrix proteins are missing or mutated. Our findings further elucidate the mechanisms of enamel formation and contribute to the efforts of developing novel enamel biomimetic materials with improved mechanical properties.

Acknowledgments

This research was supported by NIH-NIDCR R01 grants DE-13414 and DE-020099. SEM and TEM images were acquired at the Center for Electron Microscopy and Microanalysis at the University of Southern California. AFM and Raman measurements were performed at Pacific Northwest National Laboratory, which is operated by Battelle for the U.S. Department of energy under Contract DE-AC05-76RL01830. We would also like to thank Lianna Damargi for her help with the mouse dissection and sample preparations.

References

1. Lowenstam, HA.; Weiner, S. On Mineralization. New York: Oxford University Press; 1989.
2. Gao H, et al. Materials become insensitive to flaws at nanoscale: lessons from nature. Proc. Natl. Acad. Sci. U. S. A. 2003; 100(10):5597–5600. [PubMed: 12732735]
3. Addadi L, Weiner S. Interactions between acidic proteins and crystals: stereochemical requirements in biomineralization. Proc. Natl. Acad. Sci. 1985; 82(12):4110–4114. [PubMed: 3858868]

4. Kwak SY, et al. Regulation of calcium phosphate formation by amelogenins under physiological conditions. Eur. J. Oral Sci. 2011; 119(Suppl. 1):103–111. [PubMed: 22243235]
5. Qiu SR, et al. Molecular modulation of calcium oxalate crystallization by osteopontin and citrate. Proc. Natl. Acad. Sci. U. S. A. 2004; 101(7):1811–1815. [PubMed: 14766970]
6. Orme CA, et al. Formation of chiral morphologies through selective binding of amino acids to calcite surface steps. Nature. 2001; 411(6839):775–779. [PubMed: 11459051]
7. Teng HH, et al. Thermodynamics of calcite growth: baseline for understanding biomineral formation. Science. 1998; 282(5389):724–727. [PubMed: 9784126]
8. De Yoreo JJ, Wierzbicki A, Dove PM. New insights into mechanisms of biomolecular control on growth of inorganic crystals. Cryst Eng Comm. 2007; 9(12):1144–1152.
9. Herman A, Addadi L, Weiner S. Interactions of sea-urchin skeleton macro-molecules with growing calcite crystals: a study of intracrystalline proteins. Nature. 1988; 331(6156):546–548.
10. Weiner S, Addadi L, Wagner HD. Materials design in biology. Mater. Sci. Eng. C. 2000; 11(1):1–8.
11. Aizenberg J, et al. Control of macromolecule distribution within synthetic and biogenic single calcite crystals. J. Am. Chem. Soc. 1997; 119(5):881–886.
12. Berman A, et al. Intercalation of sea urchin proteins in calcite: study of a crystalline composite material. Science. 1990; 250(4981):664–667. [PubMed: 17810868]
13. Mina M, Kollar EJ. The induction of odontogenesis in non-dental mesenchyme combined with early murine mandibular arch epithelium. Arch. Oral Biol. 1987; 32(2):123–127. [PubMed: 3478009]
14. Thesleff I, et al. Epithelial-mesenchymal signaling during tooth development. Connect. Tissue Res. 1995; 32(1–4):9–15. [PubMed: 7554939]
15. Elliott, J. Structure, crystal chemistry and density of enamel apatites. In: Chadwick, DJ.; Cardew, G., editors. Dental Enamel; Ciba Foundation. first ed. John Wiley & Sons Ltd; 1997. p. 54-66.
16. Travis DF, Glimcher MJ. The structure and organization of, and the relation ship between the organic matrix and the inorganic crystals of embryonic bovine enamel. J. Cell Biol. 1964; 23:447–497. [PubMed: 14245432]
17. Orams HJ. An examination of the prism core, prism sheath and interprismatic substance using the electon microscope. Aust. Dent. J. 1966; 11(2):93–104. [PubMed: 5219045]
18. Bartlett J, Simmer J. Proteinases in developing dental enamel. Crit. Rev. Oral Biol. Med. 1999; 10(4):425–441. [PubMed: 10634581]
19. Simmer J, Fincham A. Molecular mechanisms of dental enamel formation. Crit. Rev. Oral Biol. Med. 1995; 6(2):84–108. [PubMed: 7548623]
20. Beniash E, et al. Transient amorphous calcium phosphate in forming enamel. J. Struct. Biol. 2009; 166(2):13143.
21. Llano E, et al. Identification and structural and functional characterization of human enamelysin (MMP-20). Biochemistry. 1997; 36(49):15101–15108. [PubMed: 9398237]
22. Nagano T, et al. Mmp-20 and Klk4 cleavage site preferences for amelogenin sequences. J. Dent. Res. 2009; 88(9):823–828. [PubMed: 19767579]
23. Moradian-Oldak J, et al. Controlled proteolysis of amelogenins reveals exposure of both carboxy- and amino-terminal regions. Biopolymers. 2001; 58(7):606–616. [PubMed: 11285557]
24. Kim JW, et al. MMP-20 mutation in autosomal recessive pigmented hypo-maturation amelogenesis imperfecta. J. Med. Genet. 2005; 42(3):271–275. [PubMed: 15744043]
25. Chan HC, et al. Target gene analyses of 39 amelogenesis imperfecta kindreds. Eur. J. Oral Sci. 2011; 119(Suppl. 1):311–323. [PubMed: 22243262]
26. Caterina JJ, et al. Enamelysin (matrix metalloproteinase 20)-deficient mice display an amelogenesis imperfecta phenotype. J. Biol. Chem. 2002; 277(51):49598–49604. [PubMed: 12393861]
27. Bartlett JD, et al. Decreased mineral content in MMP-20 null mouse enamel is prominent during the maturation stage. J. Dent. Res. 2004; 83(12):909–913. [PubMed: 15557396]
28. Bromley KM, et al. Amelogenin processing by MMP-20 prevents protein occlusion inside calcite crystals. Cryst. growth & Des. 2012; 12(10):4897–4905.

29. Ruan Q, et al. An amelogenin-chitosan matrix promotes assembly of an enamel-like layer with a dense interface. Acta Biomater. 2013; 9(7):7289–7297. [PubMed: 23571002]
30. Habelitz S. Materials engineering by Ameloblasts. J. Dent. Res. 2015; 94(6):759–767. [PubMed: 25800708]
31. Uskokovic V, Li W, Habelitz S. Biomimetic precipitation of uniaxially grown calcium phosphate crystals from full-length human amelogenin sols. J. Bionic Eng. 2011; 8(2):114–121. [PubMed: 22140380]
32. Ruan Q, Moradian-Oldak J. Development of amelogenin-chitosan hydrogel for in vitro enamel regrowth with a dense interface. J. Vis. Exp. 2014; 89
33. Moradian-Oldak J, et al. Self-Assembly Properties of Recombinant Engineered Amelogenin Proteins Analyzed by Dynamic Light Scattering and Atomic Force Microscopy. J. Struct. Biol. 2000; 131(1):27–37. [PubMed: 10945967]
34. Simmer JP, et al. Isolation and characterization of a mouse amelogenin expressed in Escherichia coli. Calcif. Tissue Int. 1994; 54(4):312–319. [PubMed: 8062146]
35. Wopenka B, Pasteris JD. A mineralogical perspective on the apatite in bone. Mater. Sci. Eng. C. 2005; 25(2):131–143.
36. Smith CE, et al. Relationships between protein and mineral during enamel development in normal and genetically altered mice. Eur. J. Oral Sci. 2011; 119(s1):125–35. [PubMed: 22243238]
37. Yamakoshi Y, et al. Enamel proteins and proteases in Mmp20 and Klk4 null and double-null mice. Eur. J. Oral Sci. 2011; 119(s1):206–216. [PubMed: 22243248]
38. Robinson C, et al. Dental enamel-a biological ceramic: regular substructures in enamel hydroxyapatite crystals revealed by atomic force microscopy. J. Mater. Chem. 2004; 14(14):2242–2248.
39. Rief M, et al. Single molecule force spectroscopy on polysaccharides by atomic force microscopy. Science. 1997; 275(5304):1295–1297. [PubMed: 9036852]
40. Tao J. et al. Energetic basis for the molecular-scale organization of bone. Proceedings of the National Academy of Sciences. 2015; 112(2):326–331.
41. Meldrum FC, Cölfen H. Controlling Mineral Morphologies and Structures in Biological and Synthetic Systems. Chem. Rev. 2008; 108(11):4332–4432. [PubMed: 19006397]
42. Kwak SY, et al. Role of 20-kDa amelogenin (P148) phosphorylation in calcium phosphate formation in vitro. J. Biol. Chem. 2009; 284(28):18972–8979. [PubMed: 19443653]
43. Wang L, Nancollas GH. Calcium orthophosphates: crystallization and dissolution. Chem. Rev. 2008; 108(11):4628–4669. [PubMed: 18816145]
44. Warshawsky H. Response to the critical comments on the article entitled “organization of crystals in enamel”. Anat. Rec. 1989; 224(2):264. [PubMed: 2774206]
45. Robinson C, et al. Control of crystal growth during enamel maturation. Connect. Tissue Res. 1989; 22(1–4):139–145. [PubMed: 2598665]
46. Iijima M, Moradian-Oldak J. Control of octacalcium phosphate and apatite crystal growth by amelogenin matrices. J. Mater. Chem. 2004; 14(14):2189–2199.
47. Kerebel B, Daculsi G, Kerebel LM. Ultrastructural studies of enamel crystallites. J. Dent. Res. 1979; 58(Spec Issue B):844–851. [PubMed: 283126]
48. Beniash E, Simmer JP, Margolis HC. The effect of recombinant mouse amelogenins on the formation and organization of hydroxyapatite crystals in vitro. J. Struct. Biol. 2005; 149(2):182–190. [PubMed: 15681234]
49. Yang X, et al. How amelogenin orchestrates the organization of hierarchical elongated microstructures of apatite. J. Phys. Chem. B. 2010; 114(6):2293–2300. [PubMed: 20104924]
50. Weiner S, Hood L. Soluble protein of the organic matrix of mollusk shells: a potential template for shell formation. Science. 1975; 190(4218):987–989. [PubMed: 1188379]
51. Lu JX, et al. Mineral association changes the secondary structure and dynamics of murine amelogenin. J. Dent. Res. 2013; 92(11):1000–1004. [PubMed: 24130249]
52. Moradian-Oldak J, et al. Analysis of self-assembly and apatite binding properties of amelogenin proteins lacking the hydrophilic C-terminal. Matrix Biol. 2002; 21(2):197–205. [PubMed: 11852235]

53. Tao J, et al. Roles of amorphous calcium phosphate and biological additives in the assembly of hydroxyapatite nanoparticles. J. Phys. Chem. B. 2007; 111(47):13410–13418. [PubMed: 17979266]

54. Gaume B, et al. Biomineralization markers during early shell formation in the European abalone *Haliotis tuberculata*, Linnaeus. Mar. Biol. 2011; 158(2):341–353.

55. Spoerke ED, Anthony SG, Stupp SI. Enzyme directed templating of artificial bone mineral. Adv. Mater. 2009; 21(4):425–430. [PubMed: 22068437]

56. Uskokovic V, et al. Hydrolysis of amelogenin by matrix metalloprotease-20 accelerates mineralization in vitro. Arch. Oral Biol. 2011; 56(12):1548–1559. [PubMed: 21774914]

57. Iijima M, et al. Tooth enamel proteins enamelin and amelogenin cooperate to regulate the growth morphology of octacalcium phosphate crystals. Cryst. Growth & Des. 2010; 10(11):4815–4822.

58. Fan D, et al. The cooperation of enamelin and in controlling octacalcium phosphate crystal morphology. Cells Tissues Organs. 2011; 194(2–4):194–198. [PubMed: 21525716]

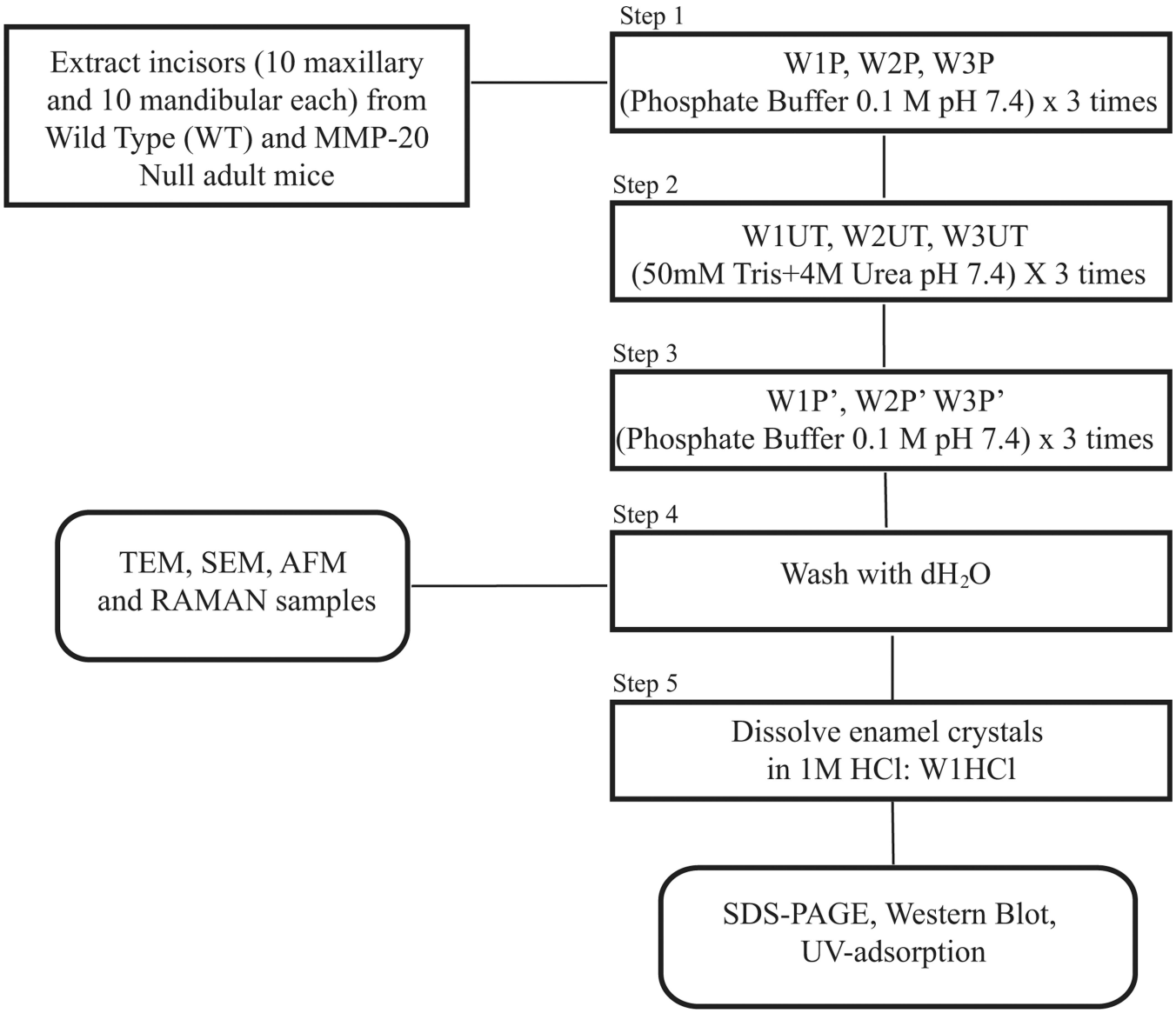

Fig. 1.

Schematic showing methods used to isolate enamel crystals from WT and MMP-20 null mice. The isolated crystals were either used for characterization experiments or dissolved in 1 M HCl for protein analysis. W1P, W2P & W3P: Phosphate buffer washes (Step 1); W2UT, W2UT & W3UT: Tris + Urea washes (Step 2); W1P′, W2P′ & W3P′: Phosphate buffer washes (Step 3); W1HCl: Dissolution in 1 M HCl (Step 5).

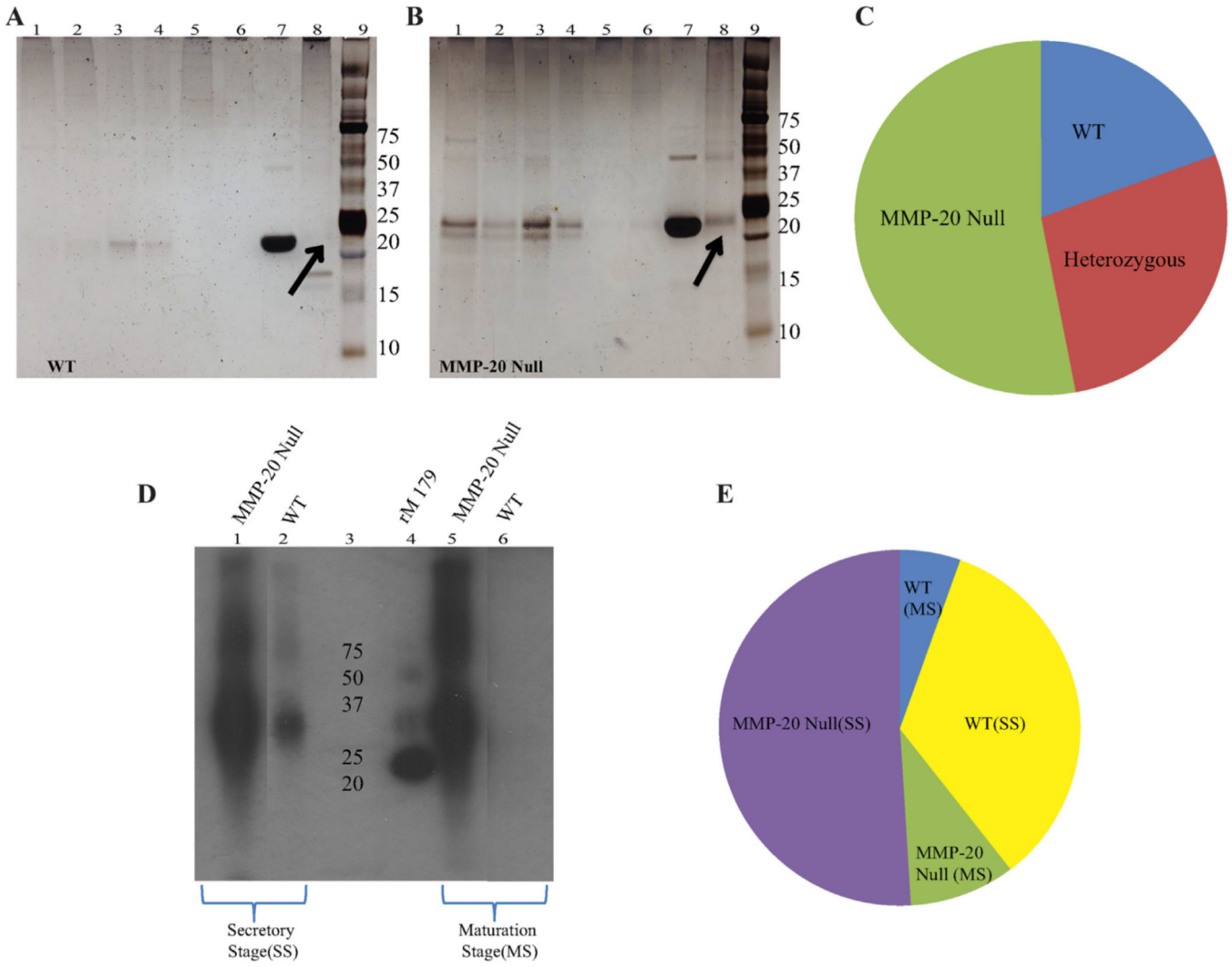

Fig. 2.

Qualitative and quantitative analysis of proteins occluded in enamel crystals (A–C: mixed secretory- and maturation-stage crystals and D–E: separated secretory- and maturation-stage crystals). A, B: SDS-PAGE of WT and MMP-20 null supernatants obtained after washing isolated enamel crystals with extraction buffers as shown in Fig. 1. Lanes: 1) W1P, 2) W2P, 3) W1UT, 4) W2UT, 5) W1P′, 6) W2P′, 7) rM 179, 8) W1HCl, 9) Protein Standard. C: Normalized amount of proteins in the samples as measured by UV-absorption obtained after dissolving the isolated crystals in 1 M HCl (W1HCl) for WT, MMP-20 heterozygous and MMP-20 null mice. D: Western blot of samples obtained from WT and MMP-20 null mice at the secretory and maturation stages. E: The normalized amount of proteins in the WT and MMP-20 null secretory- and maturation-stage enamel using UV-absorption (nanodrop).

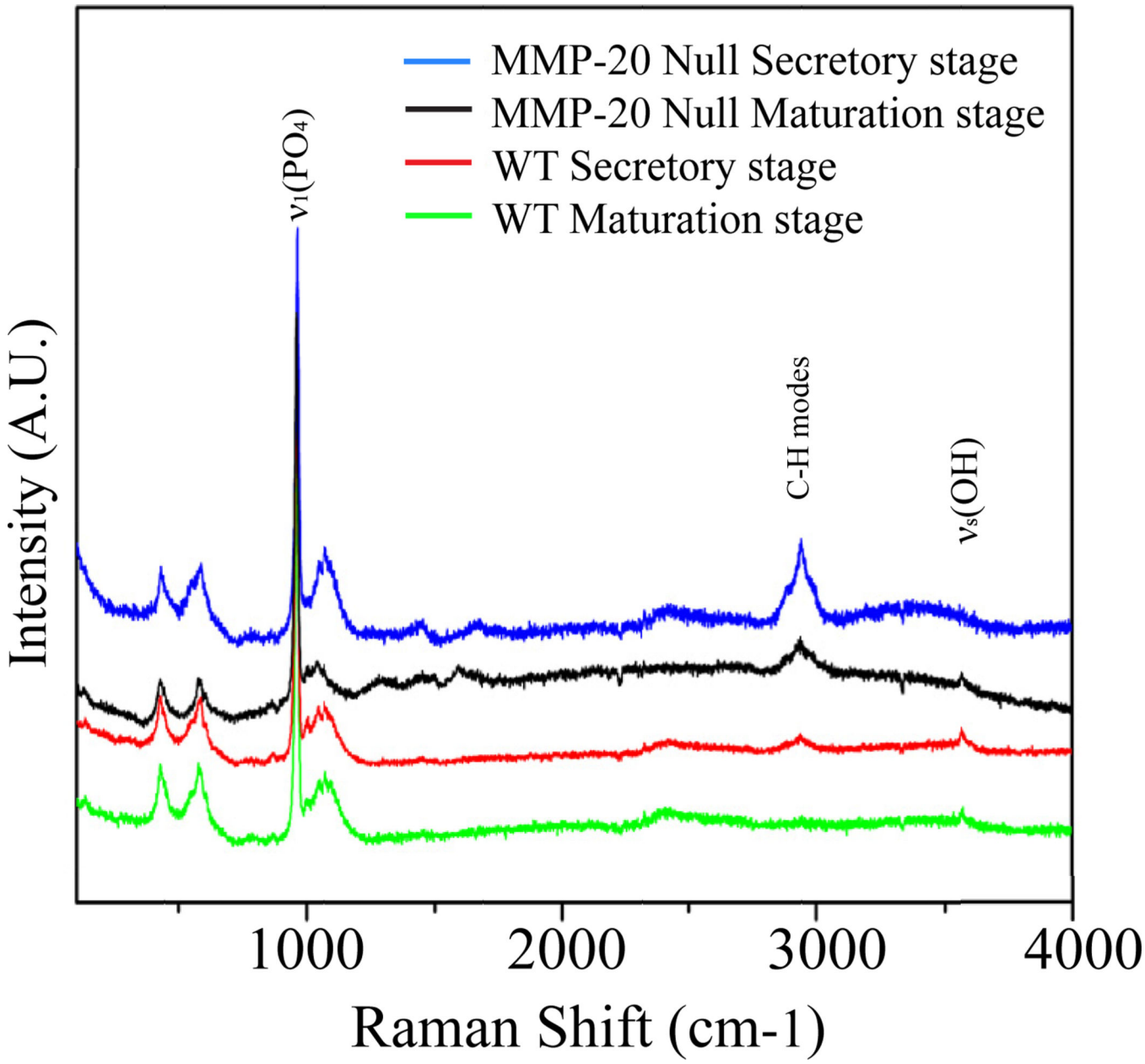

Fig. 3.

Raman spectra of WT and MMP-20 null mouse enamel crystals at secretory and maturation stages. The Raman spectra suggest that the phase of all enamel crystals is apatite. The presence of a broad peak at 3000 cm^{-1} shows the presence of a much greater amount of organic material inside MMP-20 null enamel crystals than in WT, both at secretory and maturation stages.

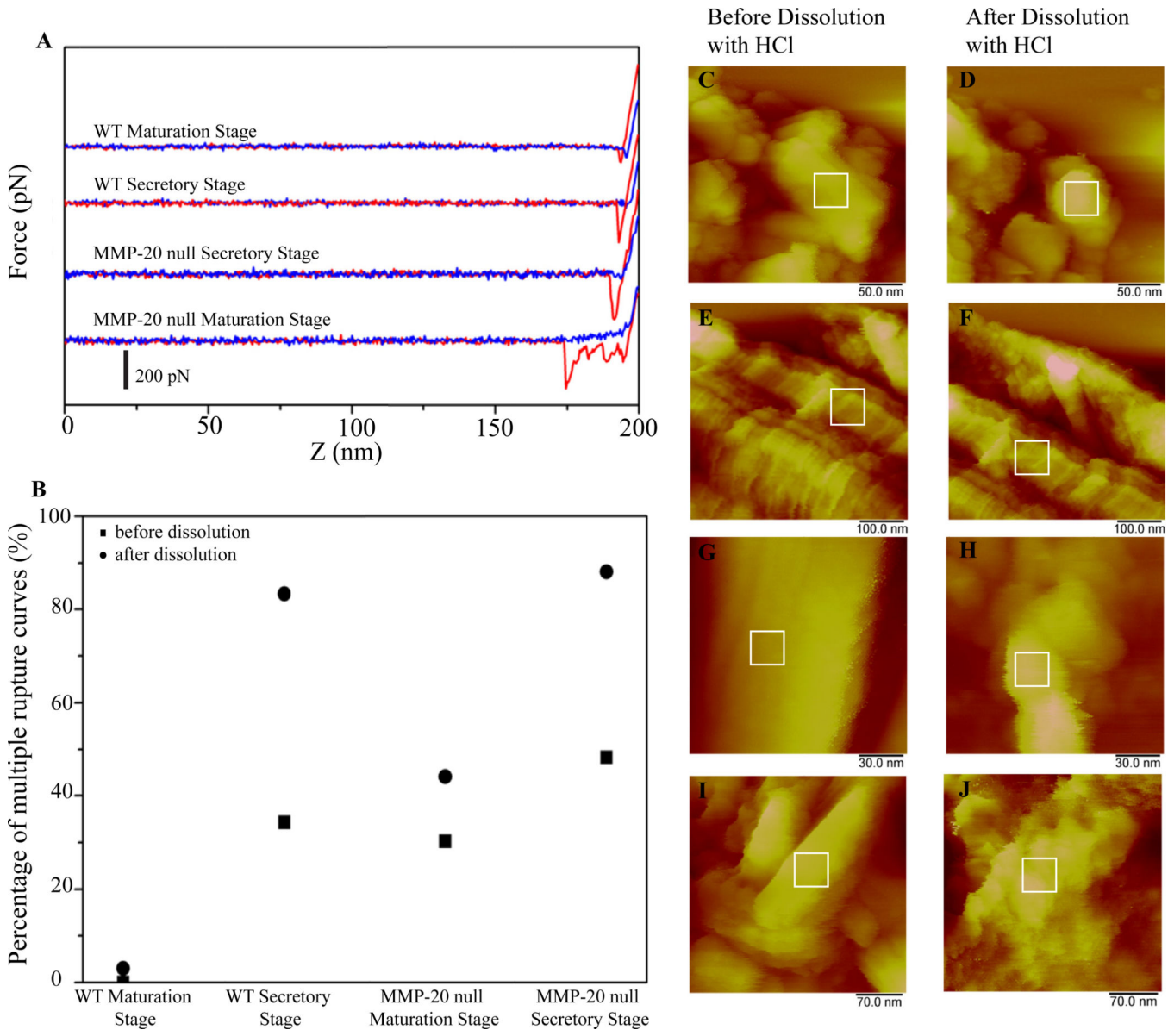

Fig. 4.

In situ AFM images and force curves of WT and MMP-20 null mouse enamel crystals at secretory and maturation stages showing single and multiple rupture curves (A). The multiple ruptures are due to the interaction between stretchable organic material and the Si_3N_4 tip. The percentage of multiple rupture force curves (B) shows the probability of the tip picking up organic macromolecules during force curve measurement before and after dissolution of enamel crystals with HCl at pH 4.6. Panels C–H show images of the following samples before and after dissolution with HCl: WT maturation (C&D), MMP-20 null maturation (E&F), WT secretory (G&H) and MMP-20 null secretory stage (I&J).

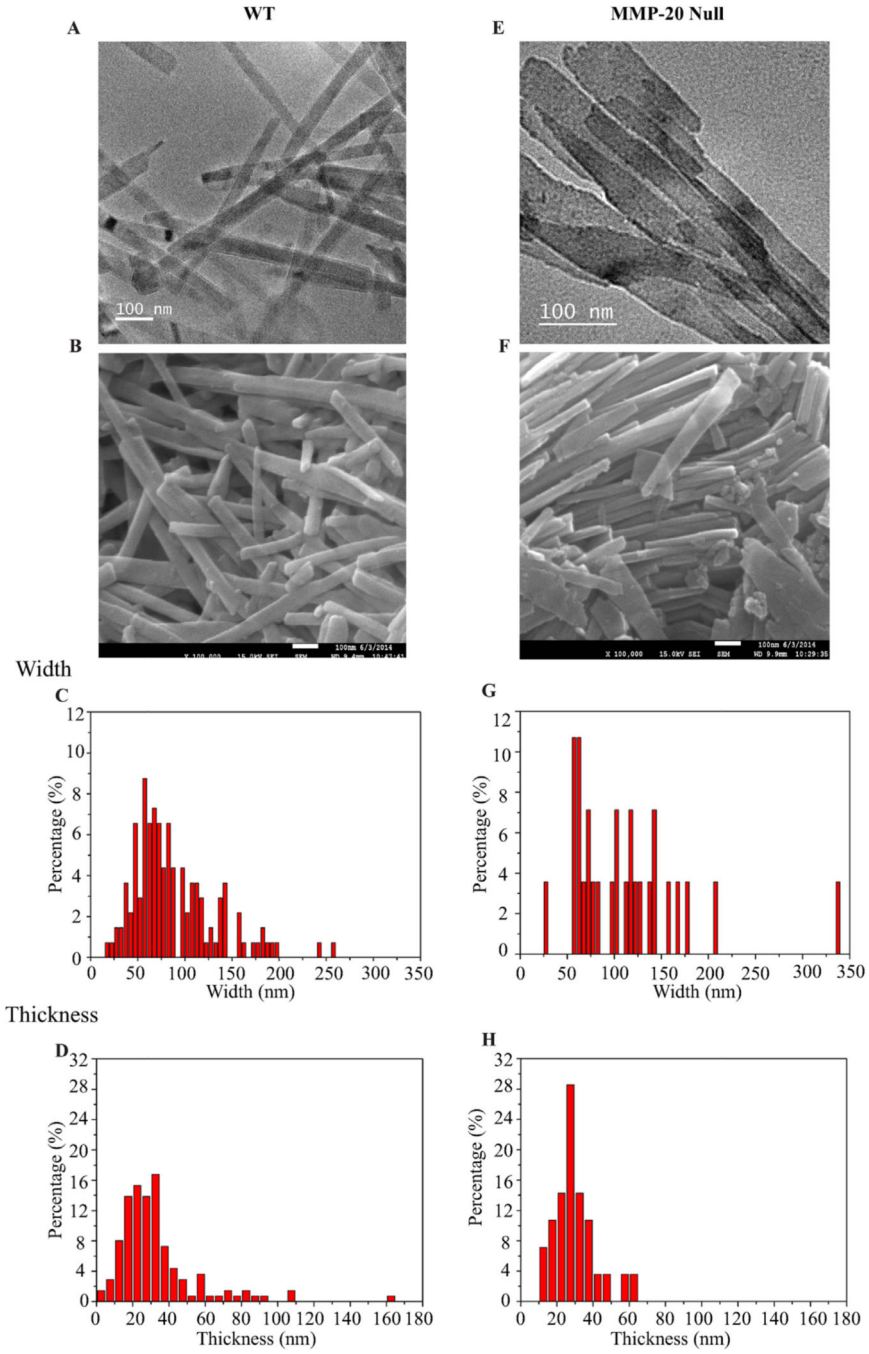

Fig. 5.

Size and morphology of isolated enamel crystals (A–D: WT and E–H: MMP-20 null mice).A, E: TEM of isolated WT (A) and MMP-20 null (E) enamel crystals. Note the difference in their length. B, F: SEM of enamel crystals isolated from WT (B) and MMP-20 (F) null mice. The enamel crystals of MMP-20 null mice are more heterogeneous, smaller in length and wider than those of the WT. C–D, G–H: Size distribution of isolated crystals from WT (C–D) and MMP-20 null (G–H) mice enamel imaged by tapping mode AFM in air. The majority of enamel crystals have a width ranging from 50 to 90 nm in WT mice

whereas the MMP-20 null enamel crystals range between 60 and 120 nm in width. MMP-20 null enamel is thinner, ranging between 10 and 30 nm, as compared to the WT, which is 20–40 nm in thickness.

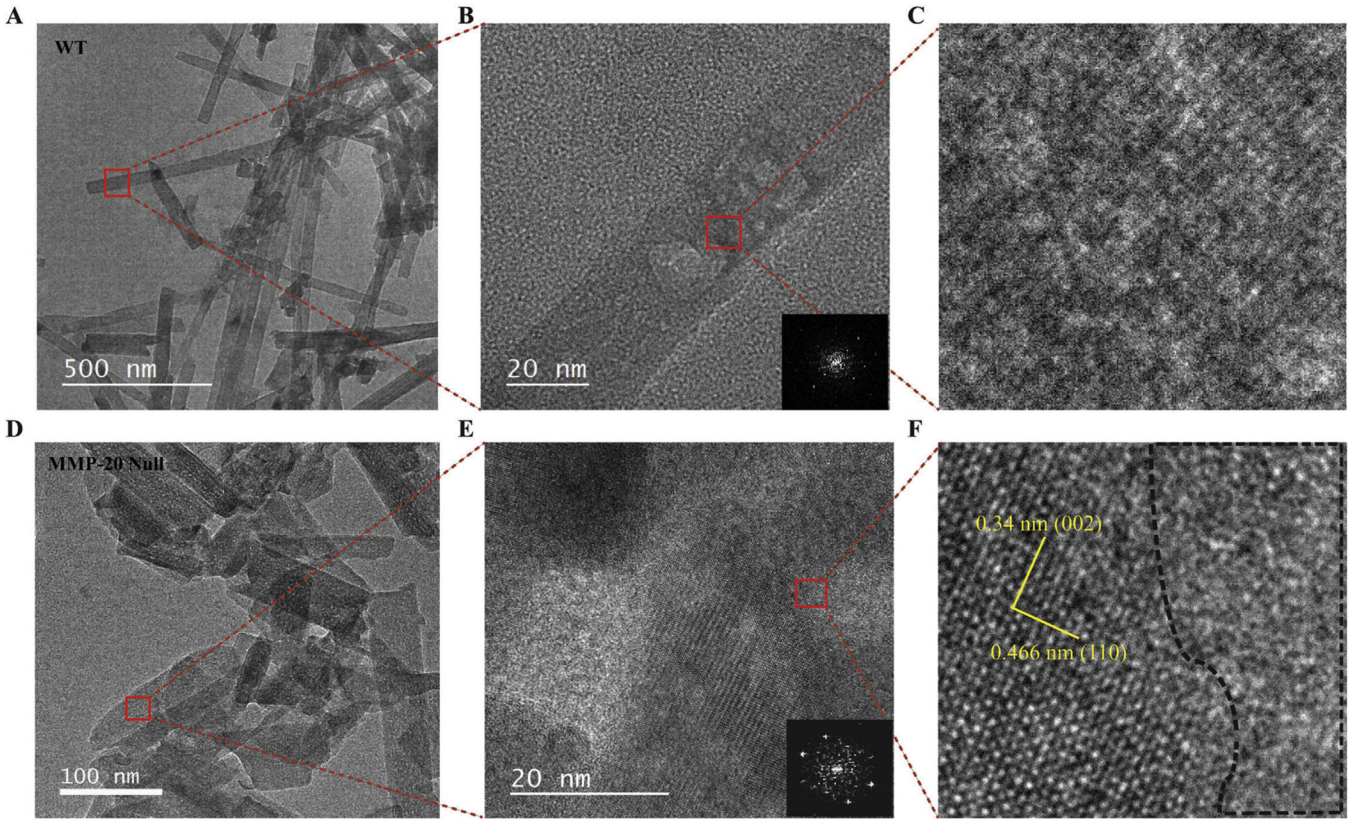

Fig. 6.

HR-TEM of WT (A, B, C) and MMP-20 null (D, E, and F) isolated enamel crystals. Fig. 7A and B shows the length of the crystals in WT and MMP-20 null mice, respectively. Figs B and E show a single crystal at a higher resolution. The insets in these panels show the diffraction patterns of marked regions as obtained by Digital Micrograph software. Figs C and F are enlarged areas (10×10 nm^2) of WT and MMP-20 null enamel crystals. The sudden loss of lattice pattern can be seen in the MMP-20 null crystals (area marked by dotted lines), indicating imperfections caused by the occlusion of enamel matrix proteins.

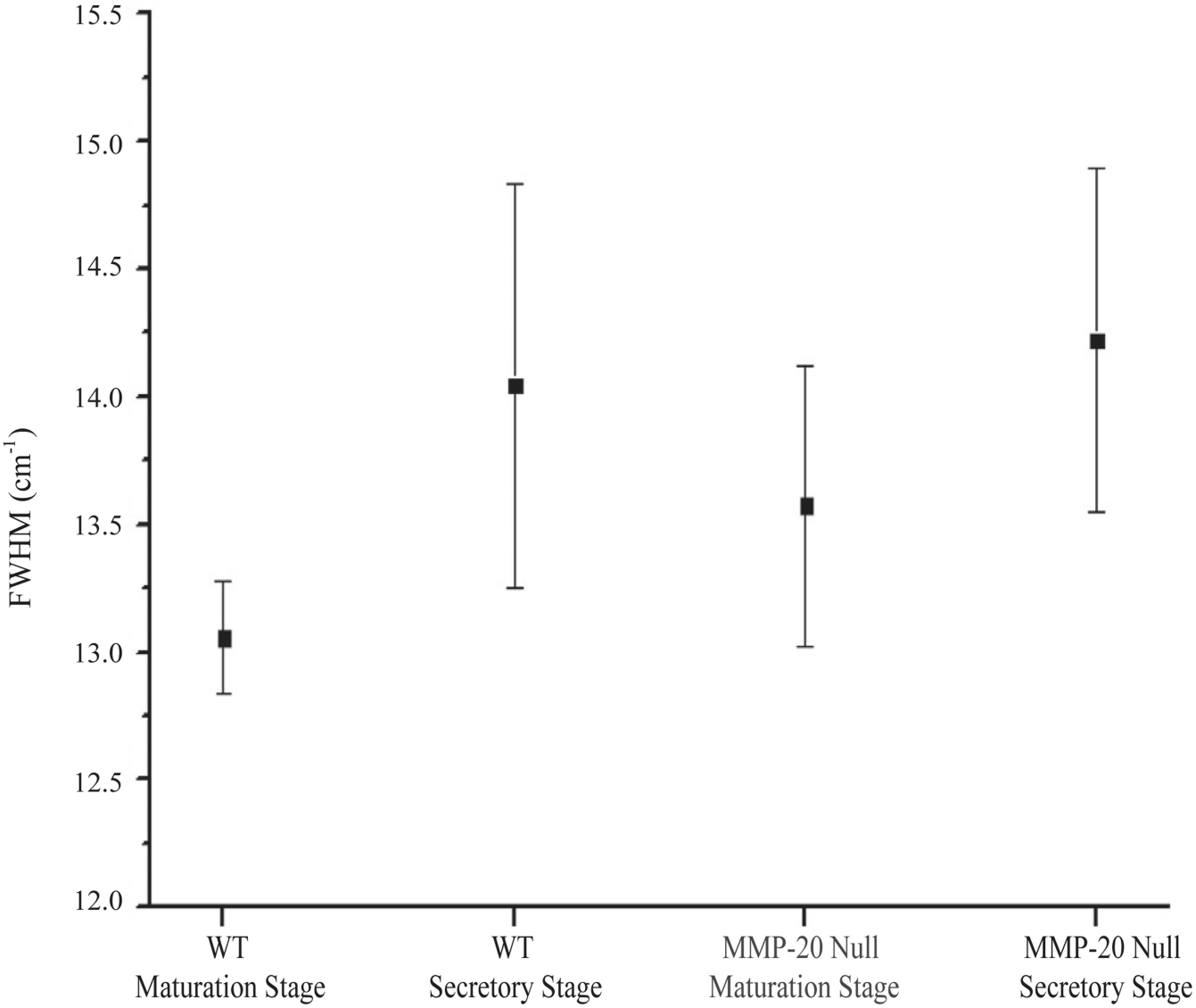

Fig. 7.

Full width of half maximum (FWHM) of peak of totally symmetric stretching mode (ν_1) of the tetrahedral PO_4 at 960 cm^{-1}. The crystallinity of WT enamel is higher (lower FWHM) than that of MMP-20 null enamel and the maturation-stage enamel is more crystalline than the secretory-stage enamel in both groups.

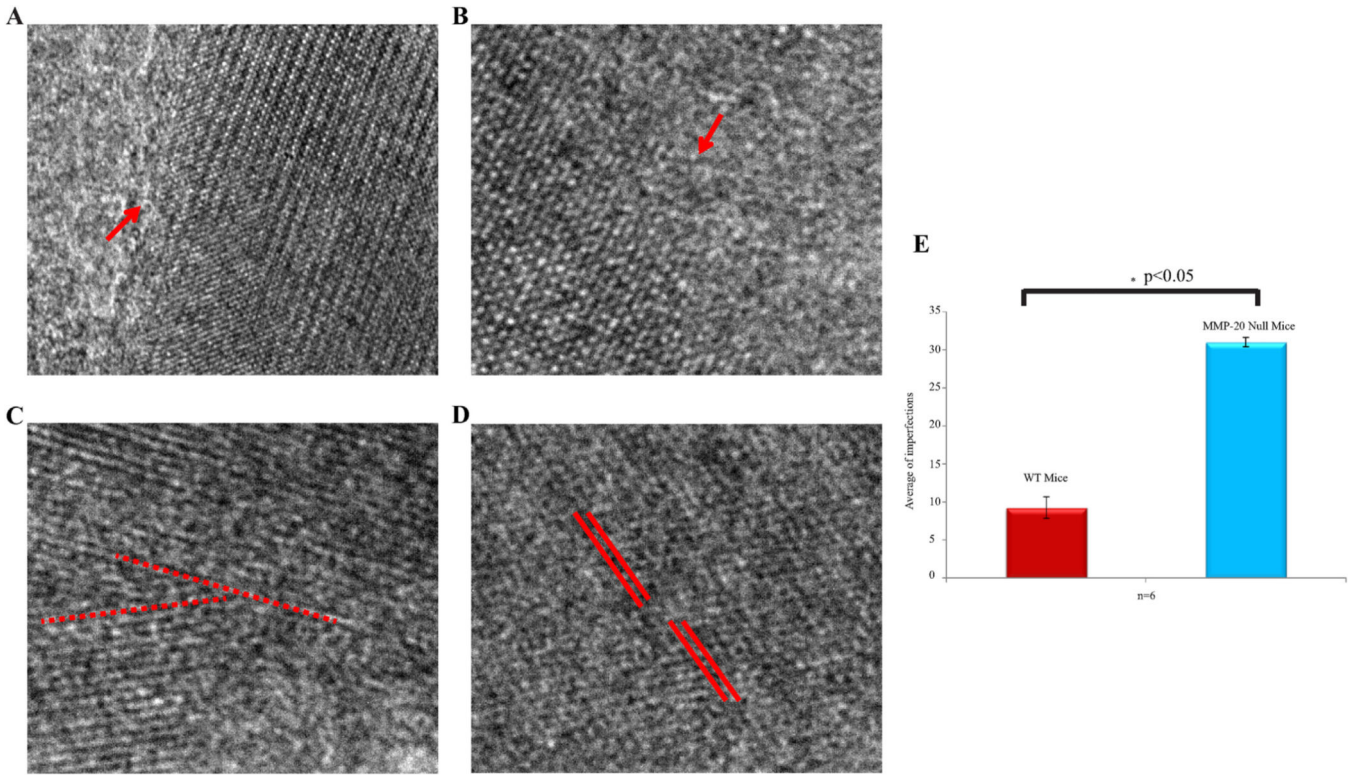

Fig. 8.

Representative HR-TEM images (10 × 10 nm^2) of imperfections found in MMP-20 null enamel demonstrating; A, B: complete absence of lattice pattern, marked by an arrow, in a single enamel crystal C, D: misalignments in lattice intervals. E: normalized areas of imperfections in the enamel crystals calculated from the HRTEM images (represented in 8 A–D) in the MMP-20 null and WT mice. The MMP-20 null enamel crystals have almost 31% imperfections as compared to 10% in WT mice.